



# Spatial eigenmodes conversion with metasurfaces engraved in silicon ridge waveguides

YAKOV GREENBERG<sup>1,2,3</sup>  AND ALINA KARABCHEVSKY<sup>1,2,3,\*</sup> 

<sup>1</sup>Electrooptics and Photonics Engineering Department, Ben-Gurion University of the Negev, Beer-Sheva, Israel

<sup>2</sup>Ilse Katz Institute for Nanoscale Science & Technology, Ben-Gurion University of the Negev, Beer-Sheva, Israel

<sup>3</sup>Center for Quantum Science & Technology, Ben-Gurion University of the Negev, Beer-Sheva, Israel

\*Corresponding author: alinak@bgu.ac.il

Received 4 March 2019; revised 17 April 2019; accepted 23 April 2019; posted 26 April 2019 (Doc. ID 361413); published 24 May 2019

We explore the discrete nature of waveguide modes and the effective medium concept to achieve an ultra-compact highly efficient mode conversion device in a high-index platform such as a silicon waveguide. The proposed device is based on a co-directional coupler that has a periodic variation in its refractive index along the propagation direction. The transverse variation of the index profile is calculated based on the interference pattern between the modes of interest. We show that mode conversion can be realized with dielectric metasurfaces engraved in the silicon waveguide. We derive the equation for effective index and show proof-of-concept numerical results of the device performance. We obtain conversion efficiencies of 95.4% between the  $TE_0 - TE_1$  modes over 8.91  $\mu\text{m}$  interaction distance and 96.4% between the  $TE_0 - TE_2$  over 6.32  $\mu\text{m}$ . The resulting coupling coefficient changes as a function of the interaction distance in a sinusoidal manner, which is crucial for constructive energy transfer from one mode to another. Such mode coupling devices have the potential for application in dispersion compensations, wavelength division multiplexing systems, and sensing. © 2019 Optical Society of America

<https://doi.org/10.1364/AO.58.000F21>

## 1. INTRODUCTION

Photonic integrated circuits (PICs) based on silicon-on-insulator (SOI) technology hold great potential in various applications such as dispersion engineering [1,2], on-chip information processing [3], chemical and biological sensors [4,5], and photonic multiplexing systems [6,7]. However, reliable, large-scale system integration of such a device still presents many challenges, including miniaturizing device footprint, increasing device operation bandwidth and robustness, and reducing device losses.

Since the bandwidth of photonic systems is limited by their optoelectronics, advanced photonic multiplexing methods may provide a solution for the growing need for high data rates. These techniques allow for multiple optical signals to be transmitted simultaneously in the same channel. The signals are differentiated based on their wavelengths [8], polarization [9], position [10], or mode profile [6] and thus, increasing the system data capacity.

The mode-division-multiplexing (MDM) method [11] employs the orthogonality principle of the different spatial eigenmodes supported by a waveguide to encode data over each separate channel. In addition, it allows for multiplexing the information over a single multimode waveguide. A key element in a MDM system is a mode converter that ideally can couple any given spatial mode into any other mode.

Conventionally, the design of mode converters relies on techniques involving integration of multiple materials [12] and complex waveguide geometries [13–15], and supports conversion between only two specific modes [16,17]. Here, we take advantage of the discrete nature of waveguide modes [18] and the effective medium concept [19] to allow the design of ultra-compact and high-efficient mode conversion devices in a high-index platform such as a silicon waveguide. Furthermore, we do not use materials other than silicon for the device, and conversion into different spatial modes is possible on the same waveguide. The proposed device is based on an all-dielectric co-directional coupler with a periodic index perturbation along the propagation direction. The transverse variation of the index profile is calculated based on the interference pattern between the modes of interest and mapped according to effective index method (EIM) to form a metasurface. Metasurfaces are artificial materials with subwavelength features that act as miniature, anisotropic light scatterers. As a result, the phase, amplitude, and polarization of light can be engineered to provide the desired optical response. Our proposed waveguide mode converter can be scaled to realize arbitrary waveguide mode conversion. As an example, we demonstrate two silicon waveguide mode converters employing all-dielectric metasurface structures that can convert  $TE_0$  mode to  $TE_1$  and  $TE_2$  modes on the same waveguide, respectively.

## 2. THEORY AND DESIGN

### A. Coupled Mode Theory

The mutual interaction between the propagating modes in an optical waveguide can be described by coupled mode theory (CMT) [18]. A finite and discrete number of orthogonal propagation modes exists in a waveguide, and in the presence of a change in the waveguide's cross section, optical modes can either couple or interfere with each other.

Our analysis is based on a 2D representation of the multimode waveguide. The electric field in the perturbed multimode waveguide can be written using the superposition of all the possible  $\mathbf{E}_m(x, y)$  eigenmodes in the unperturbed waveguide modes as

$$\mathbf{E}(x, y, z, t) = \sum_{m=1}^M A_m(z) \mathbf{E}_m(x, y) e^{i(\omega t - \beta_m z)}, \quad (1)$$

where  $m$  is the mode order,  $A_m(z)$  is the complex field amplitude (CFA),  $\beta_m$  is the propagation constant of the  $m$ th guided mode in the propagation direction, and  $\omega$  is the angular frequency.

The transverse wavefunctions  $\mathbf{E}_m(x, y)$  satisfy the unperturbed wave equation and form a complete orthonormal set, such that

$$\iint \mathbf{E}_m^*(x, y) \mathbf{E}_n(x, y) dx dy = \frac{2\omega\mu}{|\beta_m|} \delta_{mn}. \quad (2)$$

We now consider the effect of a dielectric perturbation  $\Delta\epsilon(x, y, z)$ . In the proposed device, the perturbation is implemented as a weak perturbation to the index of refraction  $n_a$  of the core of the multimode waveguide. The spatial dielectric tensor can be written as

$$\epsilon(x, y, z) = \epsilon_a(x, y) + \Delta\epsilon(x, y, z), \quad (3)$$

where  $\epsilon_a$  is the unperturbed part of the dielectric tensor, and  $\Delta\epsilon(x, y, z)$  represents the periodic dielectric perturbation along  $z$  direction. We further assume that the dielectric perturbation is weak compared to the index of the waveguide core so that the variation of the mode amplitudes satisfies the slowly varying amplitude (SVA) approximation [20]

$$\frac{d^2}{dz^2} A_m \ll \beta_m \frac{d}{dz} A_m. \quad (4)$$

Since the perturbation  $\Delta\epsilon(x, y, z)$  is chosen to be periodic in  $z$ , we can expand it into Fourier series:

$$\Delta\epsilon(x, y, z) = \sum_{k \neq 0} \Delta\epsilon_k(x, y) e^{-ik \left( \frac{2\pi}{\beta_m - \beta_n} \right) z}, \quad (5)$$

where  $\Delta\epsilon_k(x, y)$  is the  $k$ th Fourier coefficient of the perturbation, and period  $\delta$  is determined by the phase-matching condition given by

$$\delta = \frac{2\pi}{\beta_m - \beta_n}. \quad (6)$$

This is the fundamental condition where coupling between two modes can occur. It is chosen as to compensate for the propagation constant mismatch of the two modes.

Solution of the wave equation using the expressions provided above consists of a set of coupled linear differential

equations according to the number of all possible eigenmodes  $M$ :

$$\sum_m^M \frac{d}{dz} A_m = -j \sum_k \sum_n^M \kappa_{mn}^{(k)} A_n(z) e^{i(\beta_m - \beta_n - k2\pi/\delta)z}, \quad (7)$$

where  $A_m(z)$  and  $A_n(z)$  are the normalized mode amplitudes along the propagation direction  $z$ , and  $\beta_m$  and  $\beta_n$  are the propagation constants of the modes with transverse normalized electric field profiles  $\mathbf{E}_m(x, y)$  and  $\mathbf{E}_n(x, y)$ .

These coupled mode equations relate the amplitudes of each possible mode in the waveguide in terms of the phase mismatch and coupling coefficients  $\kappa_{mn}^{(k)}$  defined as

$$\kappa_{mn}^{(k)} = \frac{\omega}{4} \iint \mathbf{E}_m^*(x, y) \Delta\epsilon_k(x, y) \mathbf{E}_n(x, y) dx dy. \quad (8)$$

$\kappa_{mn}^{(k)}$  reflects the magnitude of the coupling between the  $m$ th and  $n$ th modes due to the  $k$ th Fourier components of the dielectric perturbation  $\Delta\epsilon(x, y, z)$ .

The coupling can be explained as follows. An increment in the field amplitude of the  $m$ th mode  $dA_m$  due to the coupling with the  $n$ th mode in the region between  $z$  and  $z + dz$  are related via the  $k$ th Fourier component of the dielectric perturbation.

In principle, a multiple and finite number of modes determined by the boundary conditions, material dispersion, and structure is involved. However, in practice, only two modes are strongly coupled, and Eq. (7) reduces to a set of two equations:

$$\begin{aligned} \frac{d}{dz} A_m(z) &= -j \kappa_{mn} A_n(z) e^{i(\beta_m - \beta_n)z}, \\ \frac{d}{dz} A_n(z) &= -j \kappa_{nm} A_m(z) e^{i(\beta_n - \beta_m)z}, \end{aligned} \quad (9)$$

where  $\kappa_{mn}$  is given by Eq. (8), and the reciprocity relation of the coupling coefficients is  $\kappa_{mn} = -\kappa_{nm}^*$ . Solving the coupled mode equations in Eq. (9) in the case of a co-directional coupler ( $\beta_m > 0$ ,  $\beta_n > 0$ ) and perfect phase matching, we obtain

$$\begin{aligned} A_m(z) &= [a A_m(0) + b A_n(0)] e^{-j \frac{\Delta\beta}{2} z}, \\ A_n(z) &= [a^* A_n(0) + b A_m(0)] e^{j \frac{\Delta\beta}{2} z}, \end{aligned} \quad (10)$$

where

$$\begin{aligned} a &= \left[ \cos(qz) + j \frac{\Delta\beta}{2q} \sin(qz) \right], \\ b &= -j \frac{\kappa_{mn}}{q} \sin(qz), \end{aligned} \quad (11)$$

and

$$q = \sqrt{\kappa_{mn}^2 + \left( \frac{\Delta\beta}{2} \right)^2}. \quad (12)$$

This solution would reveal a periodic exchange of power between the modes along the propagation.

### B. Design Principles

In order to efficiently couple between the  $m$ th and  $n$ th modes in a waveguide, an effective wavevector  $k_{\text{eff}}$  must be provided by the metasurface to overcome the propagation constant

mismatch. Assuming a sinusoidal perturbation, the period of the structure that allows phase matching is given by Eq. (6). However, choosing constant perturbation based on the phase-matching condition alone will cause the integral in Eq. (8) to vanish. Therefore, the perturbation  $\Delta\epsilon(x, y, z)$  must vary along  $x, y$  in order to maximize the integral in Eq. (8) coupling coefficient. Furthermore, according to the phase-matching condition, the modes will be out of phase after propagation over  $\delta/2$ . Therefore, changing the sign of  $\kappa_{mn}$  from positive to negative value is required after  $\delta/2$  to ensure constructive contribution to the conversion.

Similar to the formation of a hologram by the interference of two waves, we consider the interference of guided modes  $m$  and  $n$ . The interference pattern between the  $m$ th and the  $n$ th eigenmodes is given by

$$\mathbf{E}_m(x, y)\mathbf{E}_n(x, y)e^{-i(\beta_m - \beta_n)z} + \text{c.c.} \quad (13)$$

Based on Eq. (13), we choose a sinusoidal perturbation in the form

$$\begin{aligned} \Delta\epsilon(x, y, z) &= \epsilon_0 n_{\text{Si}} \Delta n(x, y, z), \\ \Delta n(x, y, z) &= \Delta n(x, y) e^{-i\delta z} \\ &= C_0 \mathbf{E}_m(x, y) \mathbf{E}_n^*(x, y) e^{-i\delta z}, \end{aligned} \quad (14)$$

where  $C_0$  is the amplitude of the index modulation. It is optimized through simulations in order to achieve maximal coupling efficiency over the shortest interaction distance.

Substituting Eq. (14) into Eq. (8), the coupling coefficient becomes

$$\kappa_{mn}(z) = \frac{\omega \epsilon_0 n_{\text{Si}}}{2} e^{-i\delta z} \iint C_0 |\mathbf{E}_m(x, y)|^2 |\mathbf{E}_n(x, y)|^2 dx dy. \quad (15)$$

The devices are reciprocal in terms of launching the fundamental input mode from either side of the waveguide. However, since the metasurface provides a wavevector in the direction opposite to the input, it provides a decrement in the propagation constant. Therefore, conversion from higher-order to lower-order modes is possible.

### 3. RESULTS AND DISCUSSION

The studied system is shown in Fig. 1. Conversion of waveguide modes requires preliminary information about the propagation of the eigenmodes supported by a given waveguide. Figure 2(b) shows the cross section of the proposed

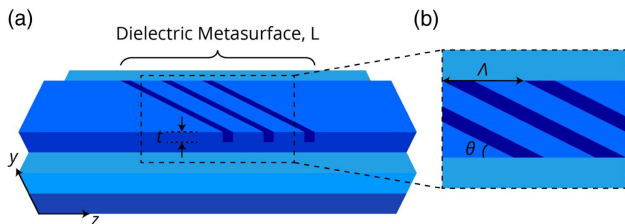


**Fig. 1.** Schematic configuration (side view) of the proposed mode converter composed from the profiled refractive index as tilted periodic slits: (a)  $L$  is the interaction distance, and  $t$  is the metasurface thickness; (b)  $\Lambda$  is the metasurface period achieved from the simulation, and  $\theta$  is the inclination angle, which is  $\theta = \tan^{-1}(2W/(j+1)\delta)$ .

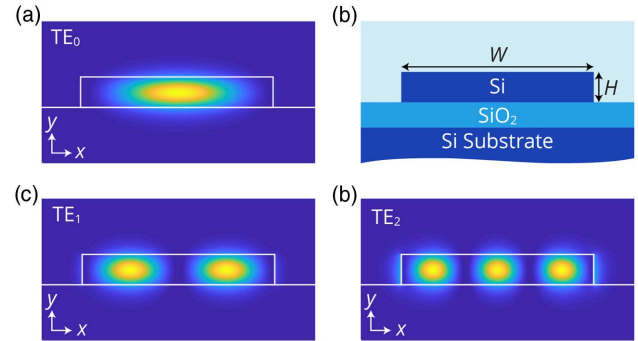


**Fig. 2.** Calculated normalized  $E_y$  component of the TE modes and structure of the proposed SOI waveguide: (a) fundamental  $TE_0$  mode, (b) schematics cross section of the studied waveguide, (c)  $TE_1$  mode, and (d)  $TE_2$  mode.

SOI waveguide strip waveguide. In our design, we use a waveguide with thickness of the top silicon layer ( $n_{\text{Si}} = 3.476$  [21]) of  $H = 200$  nm, and strip width of  $W = 1400$  nm on top of a buried oxide layer ( $n_{\text{SiO}_2} = 1.444$  [21]) operating at wavelength  $\lambda = 1.55$   $\mu\text{m}$ . To calculate the modes supported by the waveguide, we used the finite-difference-eigenmode (FDE) solver Lumerical MODE. This structure is a multimode waveguide that supports three  $TE_i$  modes that have dominant electric fields in  $\hat{y}$  direction. Figure 2(a) shows the  $|E_y|^2$  component of the fundamental  $TE_0$  mode that we use as an input to the device. We aim at converting this fundamental mode into higher-order modes of the same polarization shown in Fig. 2(c) ( $TE_1$ ) and 2(d) ( $TE_2$ ), respectively.

Figure 3 shows the 3D Finite Difference Time Domain (FDTD) simulation results of a  $TE_0 - TE_1$  mode converter. The calculated refractive index profile depicted in Fig. 3(c) is a sinusoidal modulation in both the longitudinal and transverse directions. The longitudinal period is determined based

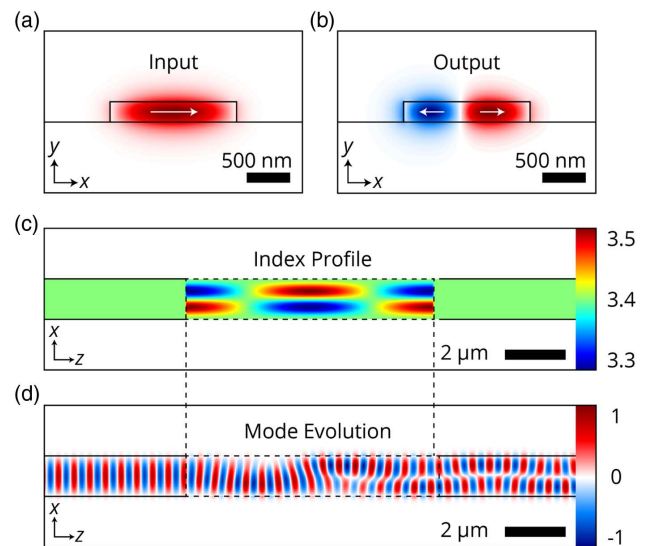


**Fig. 3.** Calculated results of  $TE_0 - TE_1$  ( $E_y$  component) mode conversion device: (a) input and (b) output mode profiles, (c) refractive index profile required for conversion, and (d) mode evolution along the propagation direction.

on the phase-matching condition, whereas the transverse profile is calculated based on 2D representation of the modes and extension of their interference pattern along the propagation direction [22]. The refractive index profile depends on the symmetry of the output mode. Odd modes produce a symmetric profile, while even modes result in an asymmetric profile. The arrows in Figs. 3(a) and 3(b) indicate the direction of the power flow.

The  $TE_0$  mode in Fig. 3(a) is launched at the input of the waveguide and propagates with no interruption. As the input mode is incident upon the metasurface, it couples and interferes with the  $TE_1$  mode as a result of the index in Fig. 3(b), resulting in energy exchange between the modes in Fig. 3(d) and the converted output mode shown in Fig. 3(b). Decomposition of the computed field on the basis of the waveguide eigenmodes allows us to determine the power transmission and crosstalk of each mode through the device [22]. Consequently, the conversion efficiency between the modes reaches 95.4% after only a single period, resulting in device length of  $L = 8.91 \mu\text{m}$ . The modulation index is  $C_0 = 0.2$  for this case.

Similar to the results presented above, we now discuss the design considerations of a  $TE_0 - TE_2$  converter. Figure 4(c) shows the calculated refractive index profile. The profile is symmetric in the  $x$  direction, since the desired output mode is odd. The treatment when considering conversion into an odd mode is similar to the previous case of an even mode. Figure 4(a) shows the input  $TE_0$ , which is incident upon the waveguide with the metasurface section; the energy is coupled out of the input mode and into the output mode gradually along the section with the perturbation [Fig. 4(d)] and finally outputs as  $TE_2$  mode [Fig. 4(b)]. The direction of power flow is depicted as arrows in Figs. 4(a) and 4(b). In this case, the conversion efficiency is 96.4% between the  $TE_0 - TE_2$  over  $6.32 \mu\text{m}$  of interaction with modulation index of  $C_0 = 0.31$ .

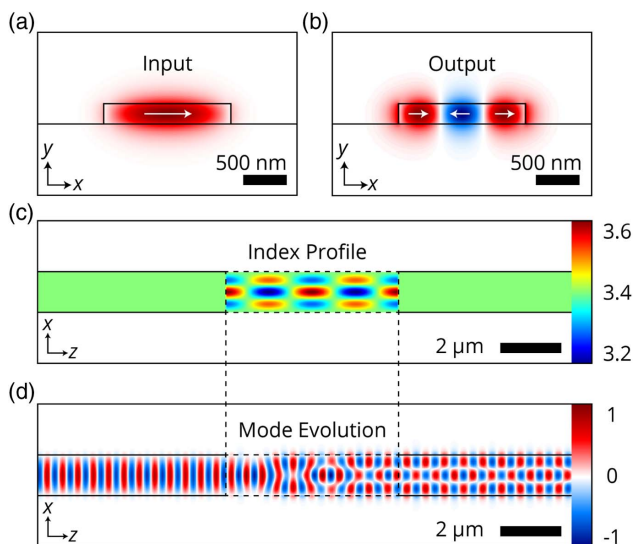


**Fig. 4.** Calculated results of  $TE_0 - TE_2$  ( $E_y$  component) mode conversion device: (a) input and (b) output mode profiles, (c) refractive index profile required for conversion, and (d) mode evolution along the propagation direction.

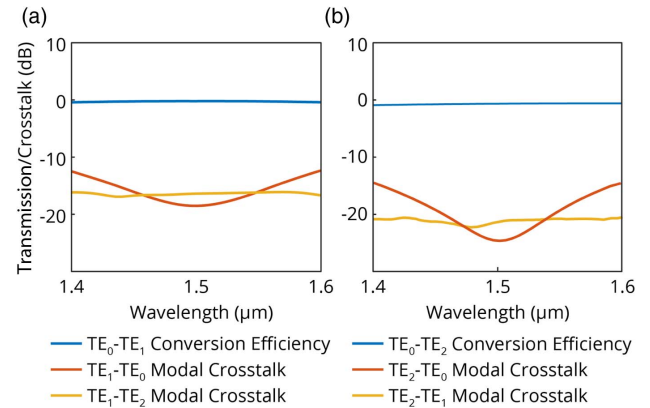


**Fig. 5.** Calculated conversion efficiency and modal crosstalk of the mode converters: (a)  $TE_0 - TE_1$  and (b)  $TE_0 - TE_2$ .

As expected, the FDTD simulations show behavior of power exchange between the modes. The refractive index profiles can be implemented as surface relief corrugations designed according to the effective medium theory (EMT). The device can be manufactured with different CMOS fabrication processes used in nanoelectronics and silicon photonics such as electron beam lithography [23,24], UV lithography [25], ionic implantation [26], and others [27–29].

Figure 5 shows the conversion efficiency and intermodal crosstalk between the modes as a function of wavelength at the output of the waveguide. The crosstalk with the input mode ( $TE_0$ ) in the  $TE_0 - TE_1$  converter reaches minimal value around the operation wavelength of  $\lambda = 1.55 \mu\text{m}$ , while the third TE mode supported by the waveguide ( $TE_2$ ) is suppressed throughout the simulated spectral range. As a result, conversion efficiency is highest at the operation wavelength and reaches 95.4%. Conversion efficiency and modal crosstalk of the  $TE_0 - TE_2$  mode converter shown in Fig. 5(b) present similar spectral behavior. The power of input mode is at its minimum at  $\lambda = 1.55 \mu\text{m}$ , and the  $TE_1$  mode is almost completely suppressed. As a result, conversion efficiency reaches 96.4%.

#### 4. CONCLUSION

To conclude, we demonstrated the mode conversion of different spatial eigenmodes on an SOI waveguide. In all examples throughout this paper, we have launched the  $TE_0$  mode to the input waveguide and built 3D-FDTD simulation to compute the electric field at the output. Compared to conventional mode-conversion devices, we converted the modes on the same waveguide using only the waveguide material. The high conversion efficiency of the devices is achieved at a relatively short interaction length. This approach of engraving metasurfaces in a material is technologically simpler compared to fabricating metasurfaces in a traditional overlayer on a waveguide as in Ref. [30]. We showed that an all-dielectric on-chip multimode conversion device can convert between  $TE_0$ ,  $TE_1$ , and  $TE_2$  modes in a silicon ridge waveguide and can be further generalized for higher-order modes. Our approach may open up the

horizons of novel chip-scale telecommunication devices such as switches, multiplexers, and many others.

**Funding.** Israeli Innovation Authority-Kamin Program, Grant. No. (62045 Year 2).

## REFERENCES

1. Y. Galutin, E. Falek, and A. Karabchevsky, "Invisibility cloaking scheme by evanescent fields distortion on composite plasmonic waveguides with Si nano-spacer," *Sci. Rep.* **7**, 12076 (2017).
2. D. Castelló-Lurbe, V. Torres-Company, and E. Silvestre, "Inverse dispersion engineering in silicon waveguides," *J. Opt. Soc. Am. B* **31**, 1829–1835 (2014).
3. Y. Shen, N. C. Harris, S. Skirlo, M. Prabhu, T. Baehr-Jones, M. Hochberg, X. Sun, S. Zhao, H. Larochelle, D. Englund, and M. Soljačić, "Deep learning with coherent nanophotonic circuits," *Nat. Photonics* **11**, 441–446 (2017).
4. A. Katiyi and A. Karabchevsky, "Figure of merit of all-dielectric waveguide structures for absorption overtone spectroscopy," *J. Lightwave Technol.* **35**, 2902–2908 (2017).
5. A. Karabchevsky and A. Kavokin, "Giant absorption of light by molecular vibrations on a chip," *Sci. Rep.* **6**, 21201 (2016).
6. L.-W. Luo, N. Ophir, C. P. Chen, L. H. Gabrielli, C. B. Poitras, K. Bergmen, and M. Lipson, "WDM-compatible mode-division multiplexing on a silicon chip," *Nat. Commun.* **5**, 3069 (2014).
7. B. Stern, X. Zhu, C. P. Chen, L. D. Tzuang, J. Cardenas, K. Bergman, and M. Lipson, "On-chip mode-division multiplexing switch," *Optica* **2**, 530–535 (2015).
8. C. A. Brackett, "Dense wavelength division multiplexing networks: principles and applications," *IEEE J. Sel. Areas Commun.* **8**, 948–964 (1990).
9. J. Wang, S. He, and D. Dai, "On-chip silicon 8-channel hybrid (de) multiplexer enabling simultaneous mode-and polarization-division-multiplexing," *Laser Photon. Rev.* **8**, L18–L22 (2014).
10. D. J. Richardson, J. M. Fini, and L. E. Nelson, "Space-division multiplexing in optical fibres," *Nat. Photonics* **7**, 354–362 (2013).
11. S. Berdagué and P. Facq, "Mode division multiplexing in optical fibers," *Appl. Opt.* **21**, 1950–1955 (1982).
12. Z. Li, M.-H. Kim, C. Wang, Z. Han, S. Shrestha, A. C. Overvig, M. Lu, A. Stein, A. M. Agarwal, M. Lončar, and N. Yu, "Controlling propagation and coupling of waveguide modes using phase-gradient metasurfaces," *Nat. Nanotechnol.* **12**, 675–683 (2017).
13. J. Zhang, T.-Y. Liow, M. Yu, G.-Q. Lo, and D.-L. Kwong, "Silicon waveguide based TE mode converter," *Opt. Express* **18**, 25264–25270 (2010).
14. D. Chen, X. Xiao, L. Wang, Y. Yu, W. Liu, and Q. Yang, "Low-loss and fabrication tolerant silicon mode-order converters based on novel compact tapers," *Opt. express* **23**, 11152–11159 (2015).
15. L. H. Frandsen, Y. Elesin, L. F. Frellsen, M. Mitrovic, Y. Ding, O. Sigmund, and K. Yvind, "Topology optimized mode conversion in a photonic crystal waveguide fabricated in silicon-on-insulator material," *Opt. Express* **22**, 8525–8532 (2014).
16. D. Ohana, B. Desiatov, N. Mazurski, and U. Levy, "Dielectric metasurface as a platform for spatial mode conversion in nanoscale waveguides," *Nano Lett.* **16**, 7956–7961 (2016).
17. W. Ye, X. Yuan, Y. Gao, and J. Liu, "Design of broadband silicon-waveguide mode-order converter and polarization rotator with small footprints," *Opt. Express* **25**, 33176–33183 (2017).
18. A. Yariv, *Optical Electronics in Modern Communications* (Oxford University, 1997).
19. J. C. Knight, T. A. Birks, P. St. J. Russell, and J. P. De Sandro, "Properties of photonic crystal fiber and the effective index model," *J. Opt. Soc. Am. A* **15**, 748–752 (1998).
20. F. Bretherton, "Propagation in slowly varying waveguides," *Proc. R. Soc. London A* **302**, 555–576 (1968).
21. E. D. Palik, *Handbook of Optical Constants of Solids* (Academic, 1998), Vol. 3.
22. A. W. Snyder and J. Love, *Optical Waveguide Theory* (Springer, 2012).
23. S. Prorok, A. Y. Petrov, M. Eich, J. Luo, and A. K.-Y. Jen, "Trimming of high-q-factor silicon ring resonators by electron beam bleaching," *Opt. Lett.* **37**, 3114–3116 (2012).
24. P. J. Bock, P. Cheben, J. H. Schmid, J. Lapointe, A. Delâge, S. Janz, G. C. Aers, D.-X. Xu, A. Densmore, and T. J. Hall, "Subwavelength grating periodic structures in silicon-on-insulator: a new type of micro-photonic waveguide," *Opt. Express* **18**, 20251–20262 (2010).
25. L. Zhou, K. Okamoto, and S. Yoo, "Athermalizing and trimming of slotted silicon microring resonators with uv-sensitive PMMA upper-cladding," *IEEE Photon. Technol. Lett.* **21**, 1175–1177 (2009).
26. M. M. Milosevic, X. Chen, W. Cao, A. F. J. Runge, Y. Franz, C. G. Littlejohns, S. Mailis, A. C. Peacock, D. J. Thomson, and G. T. Reed, "Ion implantation in silicon for trimming the operating wavelength of ring resonators," *IEEE J. Sel. Top. Quantum Electron.* **24**, 1–7 (2018).
27. A. Canciamilla, F. Morichetti, S. Grillanda, P. Velha, M. Sorel, V. Singh, A. Agarwal, L. C. Kimerling, and A. Melloni, "Photo-induced trimming of chalcogenide-assisted silicon waveguides," *Opt. Express* **20**, 15807–15817 (2012).
28. D. Bachman, Z. Chen, R. Fedosejevs, Y. Y. Tsui, and V. Van, "Permanent fine tuning of silicon microring devices by femtosecond laser surface amorphization and ablation," *Opt. Express* **21**, 11048–11056 (2013).
29. P. D. Terekhov, K. V. Baryshnikova, Y. Greenberg, Y. H. Fu, A. B. Evlyukhin, A. S. Shalin, and A. Karabchevsky, "Enhanced absorption in all-dielectric metasurfaces due to magnetic dipole excitation," *Sci. Rep.* **9**, 3438 (2019).
30. A. Karabchevsky, J. S. Wilkinson, and M. N. Zervas, "Transmittance and surface intensity in 3d composite plasmonic waveguides," *Opt. Express* **23**, 14407–14423 (2015).